

Membrane shape as a reporter for applied forces

Supplemental Material

Heun Jin Lee, Eric L. Peterson, Rob Phillips
California Institute of Technology, 1200 E. California Blvd, Pasadena, CA 91125

William S. Klug

*Department of Mechanical and Aerospace Engineering and Program in Biomedical Engineering,
University of California, Los Angeles, CA 90095*

Paul A. Wiggins*

Whitehead Institute for Biomedical Research, 9 Cambridge Center, Cambridge, MA 02142[†]

(Dated: November 19, 2008)

Contents

I. Theory	2
A. Preliminary definitions	2
B. Helfrich-Canham-Evans theory	2
C. Membrane forces in the bulk	2
D. Membrane forces at the boundary	3
E. Total force balance	4
F. Lagrange multipliers	4
G. Derivatives and thermal noise	5
II. Computational Details	5
A. Spline representation	5
B. Calculation of curvature and forces	6
C. Vesicle tracing	6
D. Proximal Equilibrium Approximation	8
1. Relation to the techniques employed by Baumart <i>et al.</i>	10
2. Applicability of the Proximal Equilibrium Approximation	11
E. Error computation for the conformational force	12
III. Experimental Details	13
1. Vesicle-induced force artifacts	13
IV. Additional Data	15
A. Lagrange multipliers	15
1. Pressure and tension	16
2. Spontaneous curvature	16
B. Other extension series	17
References	19

*Electronic address: wiggins@wi.mit.edu

[†]URL: <http://wiggins.wi.mit.edu/>

I. THEORY

A. Preliminary definitions

In these calculations, the structure of the membrane \mathcal{M} is described by a set of embedding maps $X : \mathbb{R}^2 \rightarrow \mathbb{R}^3$. We use arbitrary local coordinates σ^1 and σ^2 on the membrane. The pull-back metric on the surface is $g_{ij} = \partial_i X^\alpha \partial_j X^\alpha$ where the latin indices will refer to the coordinate system on the membrane, \mathcal{M} , and the greek indices will refer to the \mathbb{R}^3 embedding space and we use the Einstein convention (sum repeated indices). The measure on the membrane is $\sqrt{g} \equiv \sqrt{\det g_{ij}}$. The curvature is described by the shape operator, and is defined as:

$$\mathbf{S} \equiv -dX^\alpha \otimes dn^\alpha, \quad (1)$$

where d is the exterior derivative on \mathcal{M} , and n^α is the outward unit normal to the surface. The sum of the principal curvatures is the trace of the shape operator, $S \equiv \text{tr } \mathbf{S} = g^{ij} S_{ij}$, which is twice the mean curvature H , and the Gaussian curvature is the determinant of the shape operator $K \equiv \det \mathbf{S} = \frac{1}{2} \epsilon_i^k \epsilon_j^l S^{ij} S_{kl}$, where ϵ_i^k is the two-dimensional Levi-Civita symbol.

B. Helfrich-Canham-Evans theory

The membrane deformation free energy is described by the canonical theory of bilayer membranes, proposed independently by Helfrich, Canham and Evans [1–3]:

$$E = \int_{\mathcal{M}} d^2\sigma \sqrt{g} \left[\frac{1}{2} k_C (S - C)^2 + k_G K \right], \quad (2)$$

where the bending modulus k_C is typically $10 - 20 k_B T$ [4] and k_G is the Gaussian bending modulus. By the Gauss-Bonnet theorem, the second term in the bending energy $k_G K$ contributes only a topological term to the free energy and is therefore irrelevant for describing closed membranes (e.g. see Nakahara [5]). We also wish to note that the Helfrich energy is functionally identical to the Area Difference Elasticity model (ADE) up to the first variation. The effect of an area difference between the two leaflets of the membrane is to produce an effective spontaneous curvature. Incorporation of the parameter C in the Helfrich model can therefore be interpreted to include the contribution of ADE (more detail on this can be found e.g. in Seifert's review of the mechanics of fluid membranes [6]). Note that the $\frac{1}{2} k_C C^2$ term in the energy can be absorbed into the definition of the tension.

Shortly after this model was proposed, Jenkins [7] derived the Euler-Lagrange equations for the bulk of the membrane in the presence of a constant external pressure. In a companion paper, Jenkins [8] and more recently Steigmann [9] discussed more abstract models and the general constitutive relations relating force density and couple to local curvature.

C. Membrane forces in the bulk

To derive the equations for local force balance, we introduce the local Lagrange multiplier α , which represents the membrane tension. (The area of the membrane is essentially inextensible.) The constrained energy is [7, 10]:

$$E' = E + \int_{\mathcal{M}} d^2\sigma \sqrt{g} (\alpha - \frac{1}{2} k_C C^2), \quad (3)$$

where we have offset the tension by $-\frac{1}{2} k_C C^2$. We use the virtual work principle to derive the local forces (see, for example, Landau and Lifshitz [11]):

$$0 = \delta E' - \int_{\mathcal{M}} d^2s \sqrt{g} \vec{f} \cdot \delta \vec{X}, \quad (4)$$

for mechanical equilibrium where \vec{f} is an externally applied force required to cancel the elastic response, \vec{f}_{int} . The derivation of the equilibrium equations is now quite straightforward and analogous to the result found by Jenkins [7]. In the bulk of the membrane the internal elastic response force is

$$\begin{aligned} f_{\text{int}}^\perp &= S\alpha - k_C [\nabla^2 S - 2(S - C)K + \frac{1}{2}S^3], \\ f_{\text{int}}^\parallel &= 0, \end{aligned} \quad (5)$$

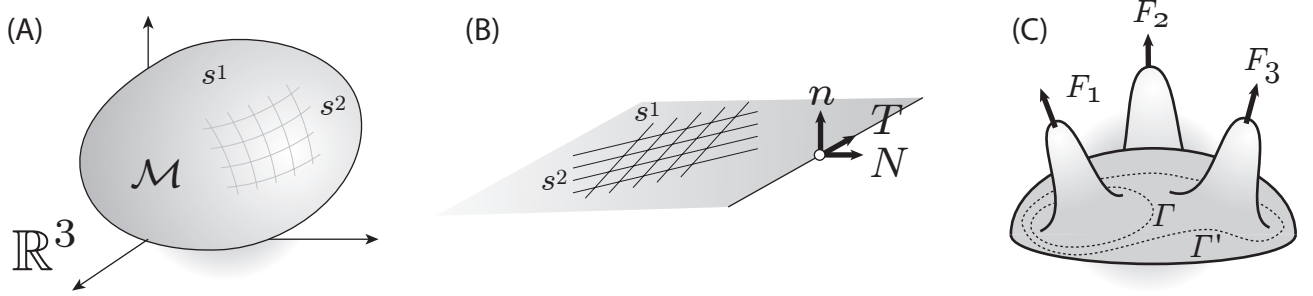


Figure S1: **Panel A:** The membrane \mathcal{M} is defined by a series of embedding maps $X : \mathbb{R}^2 \rightarrow \mathbb{R}^3$. The membrane surface is locally parameterized in the coordinates (s^1, s^2) . **Panel B:** At the boundary of the membrane $\Gamma = \partial\mathcal{M}$, we define a set of orthonormal vectors: the outward surface normal \vec{n} , the outward boundary normal \vec{N} and tangent $\vec{T} \equiv \vec{n} \times \vec{N}$. **Panel C:** A membrane with three external forces applied. Dotted lines indicated contours Γ and Γ' . The external forces in these regions can be computed with line integrals.

where ∇^2 is the Laplace-Beltrami operator or, alternatively, the two-dimensional Laplacian on the curved manifold \mathcal{M} and \perp and \parallel denote forces normal to and in the plane of the membrane, respectively. These equations reduce to those derived for constant pressure [7, 10] and are analogous to those derived for generalized theories [8, 9]. There are several points to note about these equations. Since the membrane is assumed to be fluid in-plane, the elastic response is significantly simplified. In the plane of the membrane, only potential-like forces can be supported [8], since shear forces or torques normal to the plane of the membrane will induce flow in the membrane. Furthermore, any shape can be supported by normal forces alone, resulting in a constant tension α . Consequently, we have $\vec{f}_{\text{int}} \parallel = 0$.

D. Membrane forces at the boundary

The approach for calculating these forces is exactly analogous to the calculation in the bulk. The mathematics and results in this section are well known; see, for example, Refs. [12–16]. Let us define two additional unit vectors in the plane of the membrane at the interface: \vec{N} is the outward facing normal and the tangent vector is defined $\vec{T} \equiv \vec{n} \times \vec{N}$. When these projection vectors appear as a subscript they refer to projections of vectors, tensors, or operators. For instance:

$$\nabla_N \equiv \vec{N} \cdot \vec{\nabla}, \quad (6)$$

$$S_{Ti} \equiv \vec{T} \cdot \mathbf{S} \cdot \vec{e}_i, \quad (7)$$

$$A_N \equiv \vec{A} \cdot \vec{N}, \quad (8)$$

where \vec{e}_i is the unit vector defined with respect to coordinate s^i .

When the membrane has a boundary, the principle of virtual work is

$$0 = \delta E' - \int_{\mathcal{M}} d^2s \sqrt{g} \vec{f} \cdot \delta \vec{X} - \oint_{\partial\mathcal{M}} ds \left[\vec{\mathcal{F}} \cdot \delta \vec{X} - \mathcal{L}^N \vec{n} \cdot \nabla_N \delta \vec{X} \right], \quad (9)$$

for mechanical equilibrium, where $\vec{\mathcal{F}}$ is the internal force density on the boundary and \mathcal{L}^N is the internal normal couple on the boundary required to put the membrane into mechanical equilibrium. The forces are conveniently written in terms of the membrane stress tensor. The differential force applied on the boundary of a differential region of membrane by its neighbor is

$$d\vec{F} = \vec{\mathcal{F}} ds = \vec{N} \cdot \Sigma ds, \quad (10)$$

where ds is the length of the boundary and \vec{N} is outward facing normal to the differential region (in the plane of the membrane.) See Fig. S1. The internal force density at a membrane boundary is therefore

$$\vec{\mathcal{F}}_{\text{int}} = -\vec{N} \cdot \Sigma, \quad (11)$$

and the canonical analysis leads to an expression for the internal force density

$$\vec{f}_{\text{int}} = \nabla \cdot \boldsymbol{\Sigma}. \quad (12)$$

The variational principle can be used to show that the stress tensor is

$$\Sigma^{j\alpha} = \left(\left[\frac{1}{2} k_C (S - C)^2 + \alpha \right] g^{ij} - k_C [S - C] S^{ij} \right) \nabla_i X^\alpha - n^\alpha k_C \nabla^j (S - C), \quad (13)$$

for a Helfrich membrane. The membrane couple is

$$\mathcal{L}_{\text{int}}^N = [k_C (S - C) + k_G S_{TT}]. \quad (14)$$

E. Total force balance

Noether's theorem guarantees that the total internal force and torque must cancel. (The mathematics and results in this section are well known in the literature [12–16].) The same must be true for the total external force and torque. We will develop the force cancellation explicitly since it will prove quite useful for computing external forces. The total internal force for a membrane with a boundary is

$$\vec{F}_{\text{int}} = \int_{\mathcal{M}} d^2 s \sqrt{g} \vec{f}_{\text{int}} - \oint_{\partial \mathcal{M}} ds \vec{N} \cdot \boldsymbol{\Sigma} = 0, \quad (15)$$

where we have integrated by parts to show that the forces cancel. This formalism can be quite convenient for computing external forces applied in a localized region of the membrane \mathcal{M}' . Force cancellation implies that the integrated external bulk force is equal to minus that on the boundary $\Gamma \equiv \partial \mathcal{M}'$. The total bulk external force must be equal to the total internal force on Γ :

$$\vec{F}_{\text{ext}} \equiv \int_{\mathcal{M}} d^2 s \sqrt{g} \vec{f}_{\text{ext}} = - \oint_{\Gamma} ds \vec{N} \cdot \boldsymbol{\Sigma}. \quad (16)$$

These concepts are illustrated graphically in Fig. S1. Consider a fluid lipid bilayer membrane with forces applied as shown in the Figure. The total external force F_1 applied to the membrane can be equivalently calculated as an integral over an areal region \mathcal{M}' or as an integral on the bounding contour Γ :

$$\vec{F}_1 = - \int_{\mathcal{M}'} d^2 s \sqrt{g} \vec{f}_{\text{int}} = - \oint_{\Gamma} ds \vec{N} \cdot \boldsymbol{\Sigma}. \quad (17)$$

The total external force in the region \mathcal{M}'' , bounded by contour Γ' , can be computed similarly:

$$\vec{F}_1 + \vec{F}_3 = - \int_{\mathcal{M}''} d^2 s \sqrt{g} \vec{f}_{\text{int}} = - \oint_{\Gamma'} ds \vec{N} \cdot \boldsymbol{\Sigma}. \quad (18)$$

There are two advantages to calculating the external force as a contour integral rather than an integral over an areal region:

1. The internal force \vec{F}_{int} on the boundary has been integrated relative to \vec{f}_{int} therefore it is one order lower in derivatives (third order instead of fourth order) making it more tractable numerically.
2. We may determine the external force without detailed knowledge of the structure of the membrane in the areal region; as long as the boundary has been well-determined experimentally, we may measure the force on the region internal to that boundary.

F. Lagrange multipliers

In the paper, we loosely refer to tension, pressure, and spontaneous curvature as Lagrange multipliers. In mechanics, treating tension and pressure as Lagrange multipliers is justified since the area and the volume are very close to conserved (see Fig. S8, panels A and B). (The area expansion modulus of a lipid membrane is much larger than $k_C S^2$.) The justification for treating these quantities as Lagrange multipliers in statistical physics is more

subtle. Even though the membrane is inextensible microscopically, at low tension, volume, area and curvature are hidden in thermal fluctuations leading to an entropic (rather than enthalpic) response to macroscopic area expansion. Furthermore, the spontaneous curvature is certainly not strictly a Lagrange multiplier since the total curvature is not conserved even from a purely mechanical (non-thermal) standpoint. The justification for invoking Lagrange multipliers is that they yield the same first-order variations of the energy (forces) as the rigorous theory. It is only at the second-order variation of the energy that the Lagrange multipliers fail to describe the variation of the energy correctly. For example, to calculate the fluctuations around an equilibrium configuration, the Lagrange multipliers do not suffice. An instructive example is the sphere. In the reservoir (Lagrange multiplier) theory, vesicles are unstable to radial expansion. This is the canonical nucleation problem for bubbles forming in liquid. On the other hand, if the vesicle constraints are treated correctly, these radial expansion modes are infinitely stiff in the mechanics theory.

G. Derivatives and thermal noise

One important concern about the conformational force computations that we have proposed in this paper is that these computations depend on the third derivative of the experimentally determined structure of the membrane. To what extent does experimental noise impair our ability to make force computations?

We can estimate the effect of thermal noise on the force determination in the linearized theory. If we ignore the determination of the Lagrange multipliers, it can be shown that the force sensitivity of this technique scales inversely with the spatial sensitivity. This relation arises for the same mathematical reasons as “Heisenberg Uncertainty” in wave mechanics.

The equal partition theorem predicts that the error in the integrated force due to thermal fluctuations is

$$\delta F \sim \left(\frac{2\pi^2 kT k_c \mathcal{C}}{3\ell^3} \right)^{\frac{1}{2}}, \quad (19)$$

where ℓ is the spatial resolution and \mathcal{C} is the circumference of the region of interest. We expect this expression to be an over estimate of the error since this term is the estimate of the error for the highest derivative term in the force, which is not typically the dominant term in the force. (For instance, in a tether, this term is negligible.) We can estimate the size of this error for the tethering experiments by setting the resolution equal to the radius of the region of interest:

$$\delta F \sim 0.1 \text{ pN} \times \left(\frac{k_c}{20kT} \right)^{\frac{1}{2}} \left(\frac{1 \mu\text{m}}{R} \right)^1, \quad (20)$$

which is roughly consistent with our force computations using structures determined from single images, rather than averaged structures. Higher force sensitivity can be achieved by reducing the resolution¹ of the force computation. To write this expression in a form reminiscent of the Heisenberg Uncertainty Principle, we can write:

$$\delta F \delta X \sim 0.1 \text{ pN} \mu\text{m} \times \left(\frac{k_c}{20kT} \right)^{\frac{1}{2}}. \quad (21)$$

II. COMPUTATIONAL DETAILS

A. Spline representation

We implemented the vesicle spline representation with the MATLAB command `interp1` and the `v5cubic` option. This interpolation scheme was chosen because it was convenient to implement in MATLAB. It possesses a number

¹ Reduced resolution implies increasing R .

of desirable features: (i) The cubic splines were constructed with C^2 smoothness². (ii) The interpolation method implemented by the v5cubic option makes use of basis functions with modest support³.

B. Calculation of curvature and forces

To implement the calculation of the membrane bending energy, we computed the curvatures from the spline interpolation by finite difference, then numerically integrated the energy. To compute vertex forces, we used a finite difference technique: we deformed the contour by perturbing vertices in the direction of the surface normal and then used Eq. 4 to compute the forces. To compute the integrated forces, we used the generalized Stokes theorem (Eq. 15) and a finite difference strategy of moving the membrane region, defined by the contour, by a slight amount Δz in the axial direction and computing the change in the energy ΔE , giving us a force $F = \Delta E / \Delta z$. A notable benefit of finite-difference numerical differentiation of the energy is that it helps to avoid computation of the third derivatives present in Euler-Lagrange shape equations for force density.

C. Vesicle tracing

In a typical experiment, fifty image frames were captured at each step in an extension series. An extension series usually consisted of between fifty and sixty steps, split between outward and inward movement, with a step size of roughly 1.5 μm . The integration time was chosen to give sufficient statistics to allow each frame to be traced independently. For the calculations in the main text, we constructed an average image from all the image frames at each step in the extension series. (The additional frames were captured for the analysis of the fluctuations [17].)

The vesicle conformation is represented by a cubic spline. The control points for a typical image are shown in panel A of Fig. S2. The positions of the spline control points in the direction parallel to the membrane contour were chosen by hand for each extension. We attempted a number of automated procedures for choosing the contour length positions of the points but these algorithms were difficult to implement in a robust manner.

² Continuous up to the second derivative. This property was helpful for ensuring accurate finite-difference approximation of the curvature when computing forces.

³ The interpolated curve over each segment depends on the positions of the two nearest neighboring points on each side. Other options with larger or smaller supports produced curves that differed more noticeably from the vesicle contours.

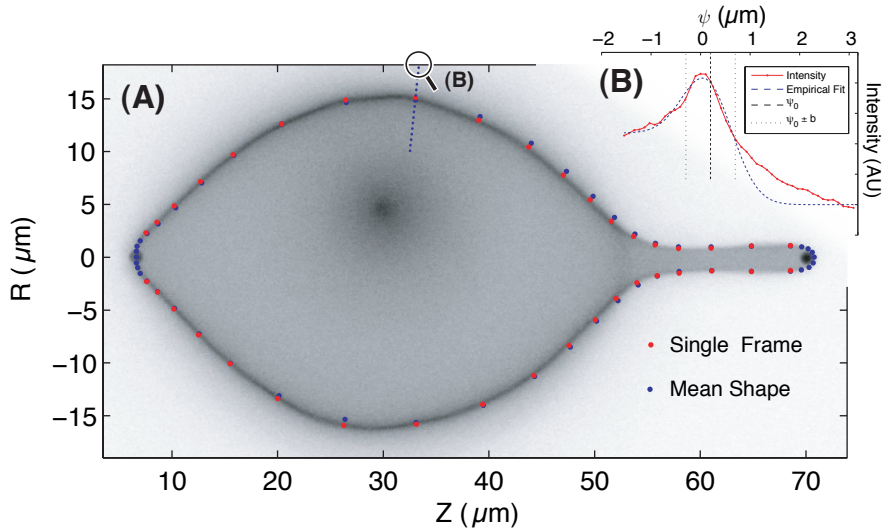


Figure S2: Capturing the membrane conformation: A fluorescence image of a vesicle from a force-extension series. The vesicle conformation is represented as a cubic spline. The positions of the control vertices are fit from the fluorescence profile. The red vertices were traced from the fluorescence image shown in the figure; the blue vertices correspond to a trace of the mean of the fifty images at this extension. The vesicle is assumed to be axially symmetric. The localized fluorescence in the body of the vesicle is the result of an internal vesicle. The increase in external osmotic pressure often leads to a budding transition. Note also that the beads are not fluorescent themselves, they appear fluorescent due to the aggregation of lipid there.

(B) Fitting control point positions. The positions of the control points normal to the contour were fit to the fluorescence profile (red curve), employing an empirical model (blue curve). The intensity values shown here were taken from a one dimensional slice of the image, shown as a blue dotted line in panel A.

The positions of the control points in the direction normal to the membrane contour were fit to the fluorescence profile, employing an empirical model. A good model for the fluorescence profile was found to be a convolution of a structure function with a Gaussian point spread function:

$$I_j(\rho; \rho_0) = \Psi_{\text{PSF}} \otimes I_0(\rho; \rho_0), \quad (22)$$

where I is the intensity at vertex j at position ρ , defined as the distance, normal to the surface, to the axis of symmetry. ρ_0 is the position of the membrane and I_0 and Ψ_{PSF} are the structure function and Gaussian point spread function respectively. The structure function is

$$I_0(\rho; \rho_0) = A\delta(\rho - \rho_0) + A\delta(\rho + \rho_0) + B\Theta_H(\rho + \rho_0)\Theta_H(\rho_0 - \rho), \quad (23)$$

where A and B are constants, δ is the Dirac delta function, and

$$\Theta_H(x) = \begin{cases} 1, & x \geq 0 \\ 0, & x < 0. \end{cases} \quad (24)$$

is the Heaviside step function. The Gaussian point spread function is defined to be

$$\Psi_{\text{PSF}}(x) = \exp(-x^2/2b^2), \quad (25)$$

where b is the point spread width. We have idealized the in-plane membrane as an infinitely thin surface, normal to the plane of focus, with a delta function source of fluorescence. The out-of-focus membrane is represented as a region of uniform intensity (the Heaviside function). A number of more elaborate (non-empirical) models were implemented but this model led to the best approximation of the observed fluorescence profile. The fit to a typical fluorescence profile is shown in panel B of Fig. S2.

In principle the force measurement should not depend on the vesicle representation (the parallel positions or number of the spline control vertices). This representation independence is shown in Fig. S3. Two independent tracings of the vesicle images show that the results for the force on the vesicle do not depend sensitively on the positions of the spline control points, as asserted.

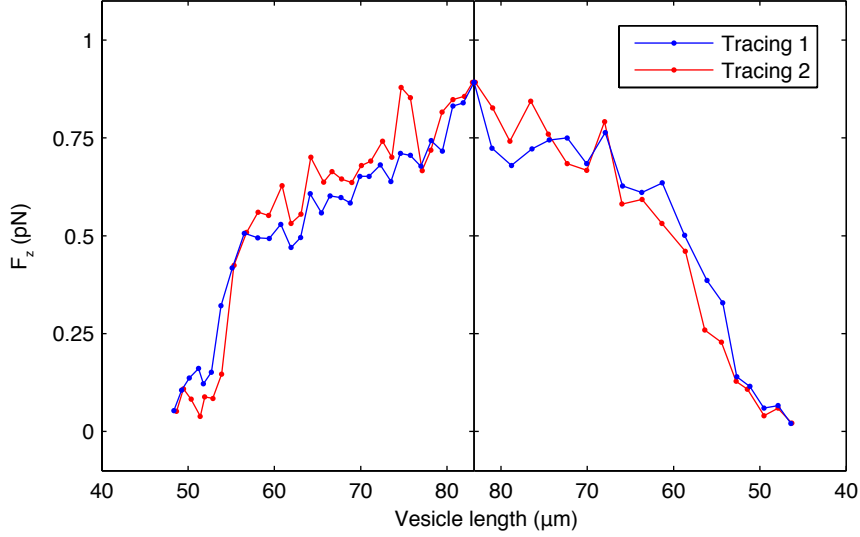


Figure S3: The conformational force is independent of the tracing representation. The figure shows two independent tracings of the vesicle extension series; the first tracing is the data shown in the text. It is clear that the two tracings are in quantitative agreement with one another, confirming that our results are not sensitive to a particular choice of spline control points.

D. Proximal Equilibrium Approximation

Analysis of the fifty image frames at each step in the extension and retraction series yielded a traced contour representing the axisymmetric shape of the vesicle. After determining the membrane structures, the Lagrange multipliers (pressure P , tension α , and spontaneous curvature C) are determined. The condition of (approximate) mechanical equilibrium was used to calculate these three multipliers.

In mechanics, there are three equivalent ways of expressing this equilibrium: at every point on the membrane (i) the energy associated with normal displacement of membrane is minimized, (ii) the force is zero, and (iii) the normal displacement to the equilibrium position is zero. Without fluctuations, all three of these statements are exactly equivalent. Therefore, for conformations that are dominated by deterministic mechanical forces rather than fluctuations, all three formulations of equilibrium should be equivalent. When fluctuations are important, one must consider the minimization of the free energy which includes the contribution from fluctuations [17].

Although these approaches for determining proximity to equilibrium appear equivalent, we argue that, from an experimental standpoint, using the normal displacements as the objective function (the “distance objective function”) is the most powerful. The first advantage of the distance objective function is that the position of vertices is determined in the experiment, not the force or energy at each vertex. It is therefore most natural to describe the experiment in terms of the observables. But most importantly, the distance objective function is least susceptible to high-frequency (short-contour-length) noise. For configurations that are close to equilibrium, the distance can be computed by multiplying the vertex forces by the stiffness matrix:

$$\psi = -K^{-1}f_{\perp}. \quad (26)$$

High frequency modes, associated with uncorrelated error in determining the positions of the vertices, can compromise the vertex forces, which depend on a fourth-order derivative of vertex position. But, the error-associated forces are canceled by the forces at neighboring vertices⁴. In essence, to determine the Lagrange multipliers, we wish to high-pass filter these forces to remove the error. Computing the estimated equilibrium displacement provides this desired filtering. High-frequency modes are stiff (have large stiffness eigenvalues) and are therefore suppressed in the estimated equilibrium displacement.

⁴ The sum of vertex forces, the integrated force, is rather insensitive to the high-frequency noise.

A particular choice of Lagrange multipliers produces a trial configuration of the membrane with control vertices displaced from their positions in the observed experimental shape. These displacements from corresponding vertices in the trial and observed membrane shapes are the estimated equilibrium displacements. To compute the Lagrange multipliers, we apply the Proximal Equilibrium Approximation: we calculate the vertex estimated equilibrium distances, ψ_i , and then minimize the sum of the squares of the equilibrium distances over the entire contour (excluding the regions near the bead attachment points) with respect to the Lagrange multipliers. (This minimization with respect to the spontaneous curvature is illustrated in Fig. S4.) The outcome of the Proximal Equilibrium Approximation analysis is the values of P , α and C as well as the forces at each vertex on the membrane, calculated solely from the shape of the membrane and the membrane bending modulus.

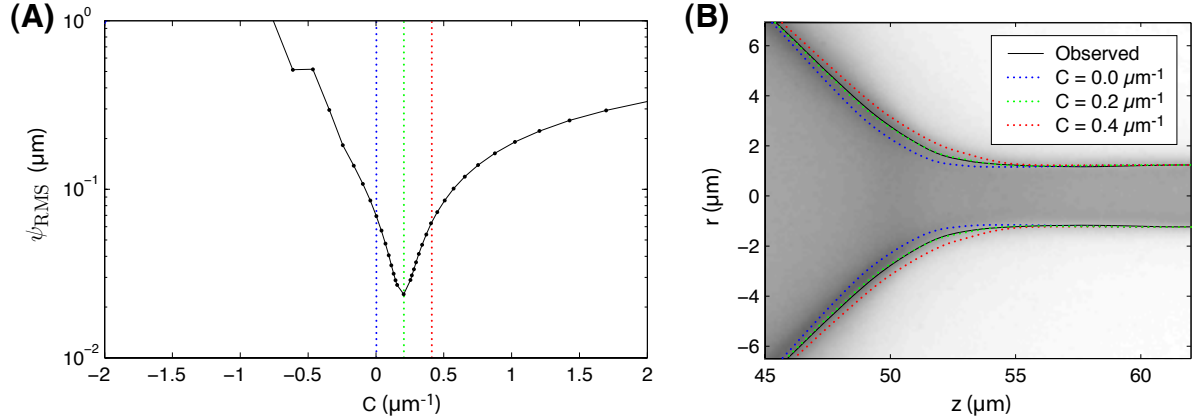


Figure S4: **The determination of C .** The Lagrange multipliers are determined by the Proximal Equilibrium Approximation: the sum of the squared equilibrium displacements (ψ_i) are minimized with respect to a three-dimensional parameter space corresponding to (α, p, C) .

Panel A. The plot shows the $\sum_i \psi_i^2$ landscape along the direction of smallest curvature, parameterized by C .

Panel B. The estimated equilibrium shape in the neck for three C values corresponding to the vertical lines in Panel A is depicted. The green curve, corresponding to $C = 0.2 \mu\text{m}^{-1}$ (close to the optimal C value), qualitatively matches the observed symmetrized conformation (black).

Step by step, the Proximal Equilibrium Approximation is carried out as follows:

1. The observed membrane shape is represented as a discretized mesh: a cubic spline with an associated set of vertices serving as anchor points. We fix the vertices near the points of contact with the trapped beads, where forces are applied.
2. We then compute the vertex forces f_i as a function of the Lagrange multipliers at each vertex i .
3. We calculate the estimated equilibrium displacement ψ_i at each vertex i . For configurations that are close to equilibrium, the distance can be computed by multiplying the vertex force by the stiffness matrix:

$$\psi = -K^{-1}f_{\perp}, \quad (27)$$

where K is the stiffness matrix computed by taking the second variation of the Helfrich energy, including Lagrange Multipliers.

4. We minimize the sum of the squares of the equilibrium displacements for all non-fixed vertices to determine the Lagrange multipliers.

Note that this algorithm is applied once to find ψ , and is not applied recursively to determine the minimal configurations. ψ is therefore a linear estimator to the equilibrium configuration. A more complete version of Fig. 2 from the main text, describing the Proximal Equilibrium Approximation, is shown in Fig. S5. Panel B shows the vertex forces for the vesicle depicted in Fig. S2. Force balance in the body of the vesicle is achieved by equilibrium between pressure and tension, whereas in the neck of the vesicle force balance is dominated by equilibrium between tension and elastic forces. The corresponding estimated equilibrium displacements are shown in Fig. S5, panel C.

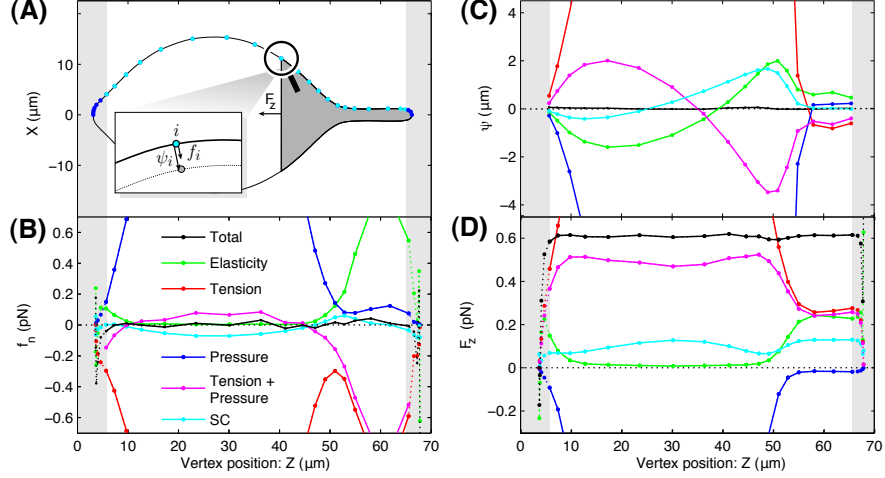


Figure S5: The Proximal Equilibrium Approximation.

(A) Vesicle conformation: The axisymmetric vesicle conformation is represented by a cubic spline. The control vertices are drawn as points along the contour. In the panel inset, we show a schematic diagram of the vertex force, f_i , the estimated equilibrium configuration (dotted line), and equilibrium displacement, ψ_i , of vertex i , defined as the normal displacement to the vertex equilibrium position (gray vertex). The summed force at vertex i , F_z^i , is the sum of the z components of the vertex forces in the dark-gray region made by excluding vertices with $z < z_i$. F_z^i is the total force applied by the right hand side of the vesicle in the z direction. In the proximity of the bead attachment points, the membrane structure cannot be resolved with sufficient precision to make reliable force estimates and these regions (light gray on the left and right of both panels) are not analyzed when solving for the pressure, tension and spontaneous curvature of the membrane with the Proximal Equilibrium Approximation.

(B) Vertex force. The vertex force f_i is the sum of components from membrane elasticity, tension, pressure, and spontaneous curvature (SC). In equilibrium, the forces should balance (up to thermal fluctuations) and indeed the total vertex force (black curve) is close to zero for the optimized Lagrange multipliers. In the body of the vesicle, force balance is dominated by tension (red curve) acting to contract the vesicle radius, and pressure (blue curve) acting to expand the radius. In contrast, in the vesicle tether, force balance is dominated by the competition between elasticity (green curve) acting to expand the tether radius, and tension (red curve) acting to contract the tether radius. The induced spontaneous curvature acts principally in the neck of the vesicle where there is a transition between the two regions.

(C) Estimated displacement to equilibrium. Although equilibrium implies force balance, it is difficult to determine the Lagrange multipliers from force balance directly since the vertex force is inherently noisy. Multiplying the vertex force f_i by the inverse stiffness matrix gives the equilibrium displacement ψ_i , the estimated spatial distance to the equilibrium configuration at vertex i . This calculation has the effect of locally averaging the vertex force and suppressing noise (and thermal fluctuations). The distance to equilibrium along the normal to the membrane surface is shown in panel C. We determine the optimal Lagrange multipliers by minimizing the sum of squares of the vertex equilibrium displacements.

(D) Summed force: The summed force is the total force applied by the right hand side of the vesicle. In equilibrium, this force can be computed from the boundary of the region; it is *independent* of the structure of the internal region. This property is of great importance since it implies that we need not resolve the region proximal to the bead attachment. The total integrated force (black) is approximately constant throughout the body of the vesicle as expected, since the forces are applied only at the poles of the vesicle. The force is also shown decomposed into individual contributions from pressure, tension, spontaneous curvature and elasticity with colors as given in panel B.

1. Relation to the techniques employed by Baumgart *et al.*

Baumgart and coworkers have also performed direct analysis of axisymmetric membrane conformation in order to determine material parameters and the line tension in multiphase vesicles [18]. In contrast, we have proposed that forces can be computed directly from membrane structure. If the pressure, tension, and spontaneous curvature are unknown, we have proposed that in some cases they may be computed by making an *ansatz* about the location of applied forces and applying the Proximal Equilibrium Approximation to determining these Lagrange Multipliers. Both PEA and the work of Baumgart *et al.* [18] determine Lagrange Multipliers by comparing the observed structure to a minimal structure.

The Baumgart strategy is to compare the minimized structure of vesicles as a function of the material parameters

to the observed vesicle structure acquired by fluorescent microscopy. The minimal vesicle structures are computed via direct integration of the axis-symmetrized Euler Lagrange equations. The observed and computed structures are fit by comparing the longitudinal-tangent angle. Clearly the proposed scope of our proposed method for conformational force computation is greater, but can the use of the PEA to determine the Lagrange Multiplier be viewed as an extension of the Baumgart *et al* technique?

Certainly from a qualitative stand point, both techniques are similar since both quantitatively analyze the observed structure. But the direct extension of the Baumgart technique presents a number of problems. (i) The Euler-Lagrange equation can only be integrated when the observed structure is axis-symmetric. For the analysis of the tethered structures, this is sufficient, although the technique that we have described can be extended to conformations without symmetry. (ii) Furthermore, the direct integration of the Euler-Lagrange equations to compute tethered vesicles is numerically problematic, as has been discussed previously [19]. In fact, the use of the Baumgart technique could only be used to analyze a small subset of the structures described in this paper. The numerics described in this paper are based finite-difference techniques which are neither limited to small deformation, nor limited to the description of axisymmetric membrane conformations.

Why does the PEA use a linear estimator to the minimal conformation instead of the minimal conformation, as described by Baumgart *et al*? (i) The linear estimators can be computed much faster than the minimal structure. For shapes close to equilibrium—small perturbations away from equilibrium, the linear estimator is sufficient. (ii) The use of the linear estimator gives a clear relation between vertices in the observed and minimized shape, implying that it is straightforward to define a measure that quantifies the distance to equilibrium.

We compare vertex positions between observed and minimal structures because the membrane position is (i) directly observed and (ii) is less susceptible to noise. The comparison of the observed and minimal structures in the Baumgart *et al.* paper is performed in terms of the longitudinal-tangent angle. For non-axisymmetric shapes, there is no unique surface tangent, but presumably this technique could be generalized using a normal, which is unique, instead of a tangent.

2. Applicability of the Proximal Equilibrium Approximation

To apply the Proximal Equilibrium Approximation, the conformation must be close to mechanical equilibrium, rather than fluctuation dominated. The key question is: are the fluctuation-induced forces larger than the mechanical forces that result in the mean conformation? Theoretical calculations⁵ suggest that this question is resolution dependent but that structures that are reproducible (not fluctuation dominated) do give meaningful results when the Proximal Equilibrium Approximation method is applied. The effect of thermal fluctuations on the consistency of the Proximal Equilibrium Approximation can be tested directly: we generated membrane tracings from both individual image frames as well as from the mean of the fifty images at each step in the extension/retraction series. The analysis of traces from individual image frames results in a distribution of force measurements whose mean can be taken as the value of the force at that step in the experiment. The mean force from the 50 individual tracings varied by an average of 0.07 pN from the value of the force calculated from the traced average image, a value that is small in comparison with other sources of error in the experiment.

A second limitation of the Proximal Equilibrium Approximation is the approximate degeneracy of some membrane conformations with respect to the Lagrange multipliers. Perhaps the most obvious example is the sphere. The Proximal Equilibrium Approximation essentially solves for the Lagrange multipliers by balancing the elastic and constraint forces. For the sphere, there are no elastic forces to balance⁶. Since the elastic forces vanish, there is a two-dimensional continuum of Lagrange multipliers that satisfy the force balance equations. Obviously, the sphere is a special case, but shapes at the tethering transition point appear to have only a weak dependence on the spontaneous curvature. Uncertainties in the spontaneous curvature appear to dominate the error in conformation force computation. (See Fig. S8.)

A final limitation of the Proximal Equilibrium Approximation is the necessity of guessing and excluding points where external forces are applied when computing the Lagrange multipliers. While the location of the applied forces is obvious in the analysis of deformed vesicles, for biological examples, the position of the applied forces may not be known. Indeed, in many examples, the contacts may be so frequent as to not permit large, force-free regions to be

⁵ By perturbing around a flat configuration, we can analyze the contribution of thermal fluctuations to the measured forces. As the resolution of the vertex grid is increased, the force resolution is reduced.

⁶ The fact that the elastic force vanishes for the sphere isn't obvious. The easiest way to see this is to compute the elastic energy of a sphere. In the energy, the factors of R (the radius) from the area and curvature cancel leading to an energy that is scale independent. The radial forces are therefore zero.

identified and analyzed⁷. On-the-other-hand, in biological applications, the pressure can be completely neglected and the tension and spontaneous curvature may be regulated by the cell or determined using other techniques [20]. If the Lagrange multipliers are known, it is straightforward to compute membrane forces without applying the Proximal Equilibrium Approximation.

E. Error computation for the conformational force

The error in the force computed from the conformation of the membrane was estimated in two ways in our analyses. One method consists of tracing each of the 50 images at each step in the extension/retraction series, applying the Proximal Equilibrium Approximation and then analyzing the resulting distribution of force, pressure, tension and spontaneous curvature measurements. This is the method used to generate the r.m.s. errors on the force shown in the main text.

Another method consists of calculating confidence intervals for the Lagrange multipliers and then deriving the error in the force based on those uncertainties. This can be done by standard methods; see, for example, Bevington and Robinson [21], whose analysis we follow here. The Proximal Equilibrium Approximation amounts to a non-linear least squares fit of the membrane contour given values for the pressure, tension and spontaneous curvature to the observed membrane contour. The χ^2 goodness-of-fit parameter in the Proximal Equilibrium Approximation is:

$$\chi^2 = \sum_i \frac{1}{\sigma_i^2} [y_i - y_{\text{obs}}]^2, \quad (28)$$

where σ_i is the uncertainty in the position of vertex i in the direction normal to the membrane contour, y_{obs} is the observed position of the vertex in the normal direction and y_i is the position of the i th vertex given parameter values P , α and C . The uncertainty in the normal positions, σ_i , was essentially constant for each of the vertices in a given image from our experiments. In the neighborhood of the minimum χ^2 value found by the Proximal Equilibrium Approximation, we may use a Taylor expansion of our fitting function, y_i , to find:

$$\Delta a_j = \epsilon_{jk} \beta_k \quad (29)$$

where Δa_j is the uncertainty on the j th parameter, ϵ_{jk} is the error matrix and β_k is the derivative of χ^2 with respect to the k th parameter. This was the technique used in generating the errors shown as dotted lines on the plots of pressure, tension and spontaneous curvature in Fig. S8 below. More generally, after finding the optimal point in χ^2 space, we may calculate the χ^2 values in the neighborhood of this point and find contours in parameter space where χ^2 increases by a given amount to find arbitrary confidence intervals on the parameters. We found that using the χ^2 method of estimating confidence intervals on the parameters predicted larger errors than the r.m.s. method from the 50 images at each step in the experiment.

⁷ In the experiments described in this paper, the deformation incurred by tethered vesicles is so large that the body of the vesicle cannot be treated as a reservoir with constant Lagrange multipliers. In most biological systems of interest, the size of the remodeled regions is small in comparison with the size of the cell. For cellular-scale membrane deformations, membrane force computations are unlikely to be of interest since it is not the membrane mechanics which dictates the shape, but the underlying structure of the cytoskeleton.

III. EXPERIMENTAL DETAILS

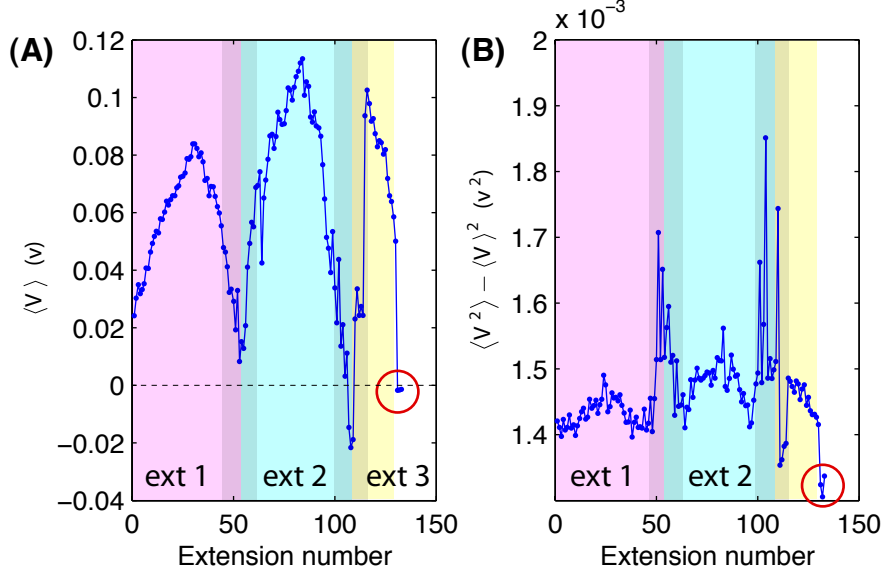


Figure S6: **Panel A:** The mean PSD voltage plotted versus extension number for a three extension data set. The trap deflection (and force) are proportional to the PSD voltage. The last three circled points are the zeros for the experiment with beads unattached to the vesicle. The initial points on the trace correspond to beads bound to the vesicle, but without extension. Binding the vesicle causes an anomalous force due to scattering of light. See discussion in the caption of Fig. S7. **Panel B:** The voltage variance versus extension number. The voltage variance is inversely proportional to the trap stiffness. Note first that the voltage variance is stable relative to its magnitude throughout the extension. (The data has been plotted to accentuate variations by not including zero on the y axis.) As the force is increased in the first extension, the voltage variance is increased slightly, corresponding to a slight reduction in the trap stiffness, as would be expected due to the large-deflection non-linearity in the trap. Two larger features are visible in the voltage variance at extension numbers 65 and 110. These features are the result of changes in the local structure of the vesicle surrounding the bead. See discussion in the caption of Fig. S7.

1. Vesicle-induced force artifacts

Although the vesicle does not significantly affect the trap stiffness, it does affect the DC offset of the PSD. If the trap is zeroed without contact with the vesicle, the presence of the vesicle in the beam scatters light, leading to an offset voltage at the PSD. It was therefore necessary to assume a zero on bead contact. The beads were bound to the membrane by squeezing the vesicle between the trapped beads.

We also discovered that changes in the vesicle conformation in proximity to the bead could also lead to force artifacts. The evidence for this effect is discussed in Fig. S7. Data sets where the vesicle tethered on the pole opposite from the force sensor did not appear to show these anomalous forces, presumably because the local vesicle conformation was not appreciably changed by deformation.

We also note that the trapping force is susceptible to drift in the sub-piconewton regime. Due to the competing effects of drift and systematic uncertainties related to membrane-induced beam scattering, the most meaningful comparisons between the conformational force and the trapping forces are differences between conformations separated by a few extension steps since the membrane-induced scattering is similar and the drift between adjacent steps is smaller than between measurements taken ten to twenty minutes apart. As a practical matter of reducing the influence of drift and low-tension vesicle structure induced force anomalies, the DC offset was calculated by minimizing the difference between the trapping force and conformational force at high force.

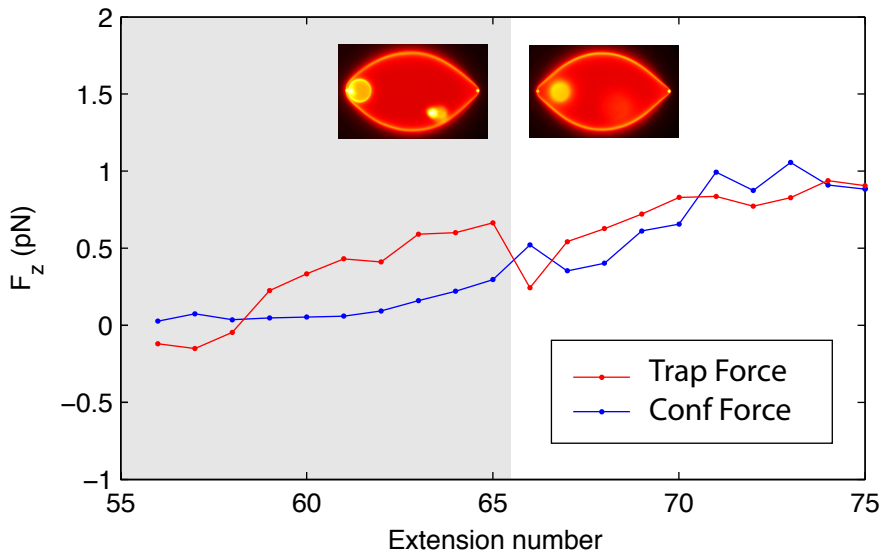


Figure S7: **A limitation of measuring trap forces in the presence of a vesicle.** The vesicles themselves scatter the trapping beam, which can result in the detection of anomalous forces. In the figure above, we depict the most compelling evidence for this effect. At the beginning of this data set, an internal vesicle is bound to the lipid aggregate surrounding the bead. Between extension numbers 65 and 66, the vesicle is released and diffuses into the body of the outer vesicle. This release causes a precipitous drop in the detected trap force (black curve). For reference purposes, we have also plotted the force calculated from the membrane conformation (blue curve). A similar offset in force is observed upon attachment of the force detection bead to the vesicle. Rigorously, this implies that at best we can detect relative forces, not absolute forces. Similar anomalies occur when the vesicle becomes tethered at the detection bead, due to a dramatic change in local vesicle structure. The most reliable force traces resulted from vesicles tethering at the extension bead. In spite of these complications, the trap stiffness was not significantly affected by the vesicle.

IV. ADDITIONAL DATA

In this section, we provide a more extensive presentation of the experimental data. We present both the vesicle structures and the Lagrange multipliers computed for the extension series shown in the main text. In Section IV B, we present force-extension data from other vesicle extension series.

In Fig. S8, we show a complete set of traced membrane conformations for the vesicle force extension curve discussed in the main text. Under extension, the vesicle undergoes a shape transition to a tethered conformation. The body of the vesicle is supported by tension-induced contractive forces which balance the outward force of pressure. But, as the radius of curvature shrinks at the tether neck, the tension forces increase as R^{-1} , overcoming the outward pressure. The tether neck radius shrinks until the outward-acting elastic force, which scales like R^{-3} , stabilizes the conformation. This force cancellation is illustrated explicitly in Fig. S5 in Section IID.

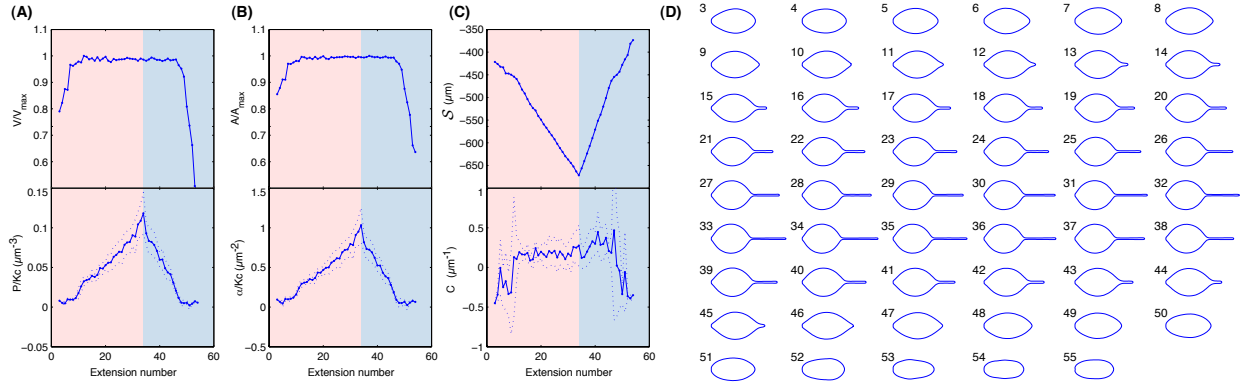


Figure S8: Tension, pressure and spontaneous curvature of a tethered vesicle. In this figure we plot the estimated pressure p , tension α and spontaneous curvature C as a function of extension number for an extension (pink region) and contraction (blue region) of a vesicle. The volume V , area A and integrated curvature S are also shown. **Panels A and B:** In the top panes of Panels A and B, the apparent volume and area of the mean conformation are plotted versus extension number. The volume and area of the membrane are fixed, therefore the change in apparent volume and area upon extension and contraction is the result of volume and area hidden in fluctuations from the mean, cylindrically-symmetric conformation. In the lower panes of Panels A and B, the vesicle pressure and membrane tension are plotted versus extension number as determined by PEA, respectively. The pressure and tension rise steadily with tether extension and are peaked, as expected, at the maximum extension.

Panel C: The Integrated curvature and spontaneous curvature as a function extension number. The spontaneous curvature is predicted to be a linear function of the integrated curvature by the ADE theory. This linear relationship is not observed and explanations for the failure of the ADE model to predict the spontaneous curvature are discussed in the text.

Panel D: The vesicle conformations. In the figure above we show the symmetrized mean vesicle conformations with the corresponding extension numbers for the data analyzed in the text.

A. Lagrange multipliers

As described in Sect. IID, the Lagrange multipliers for each configuration are determined by applying the *Proximal Equilibrium Approximation*. Although we refer to these quantities as Lagrange multipliers, they have a simple physical interpretation: P , α , and C are the pressure, tension, and spontaneous curvature respectively. From a macroscopic mechanics perspective, the pressure and tension are essentially constraint forces since the membrane area and volume are essentially inextensible at the forces applied in this experiment. Spontaneous curvature is more subtle. Two important effects contribute to the spontaneous curvature: (i) the number of lipid molecules in each leaflet relative to the leaflet area, and (ii) asymmetries in the composition or solvent environment of the two leaflets. The *Area Difference Elasticity* model (ADE) describes how the leaflets expand and contract in order to accommodate the area difference between bilayers [6]. We found that the values of all three of the Lagrange multipliers evolved with the vesicle conformation. These results are shown in Fig. S8 where the Lagrange multipliers are plotted as a function of the extension number. In Fig. S9, we plot the effective constitutive relations for the vesicle.

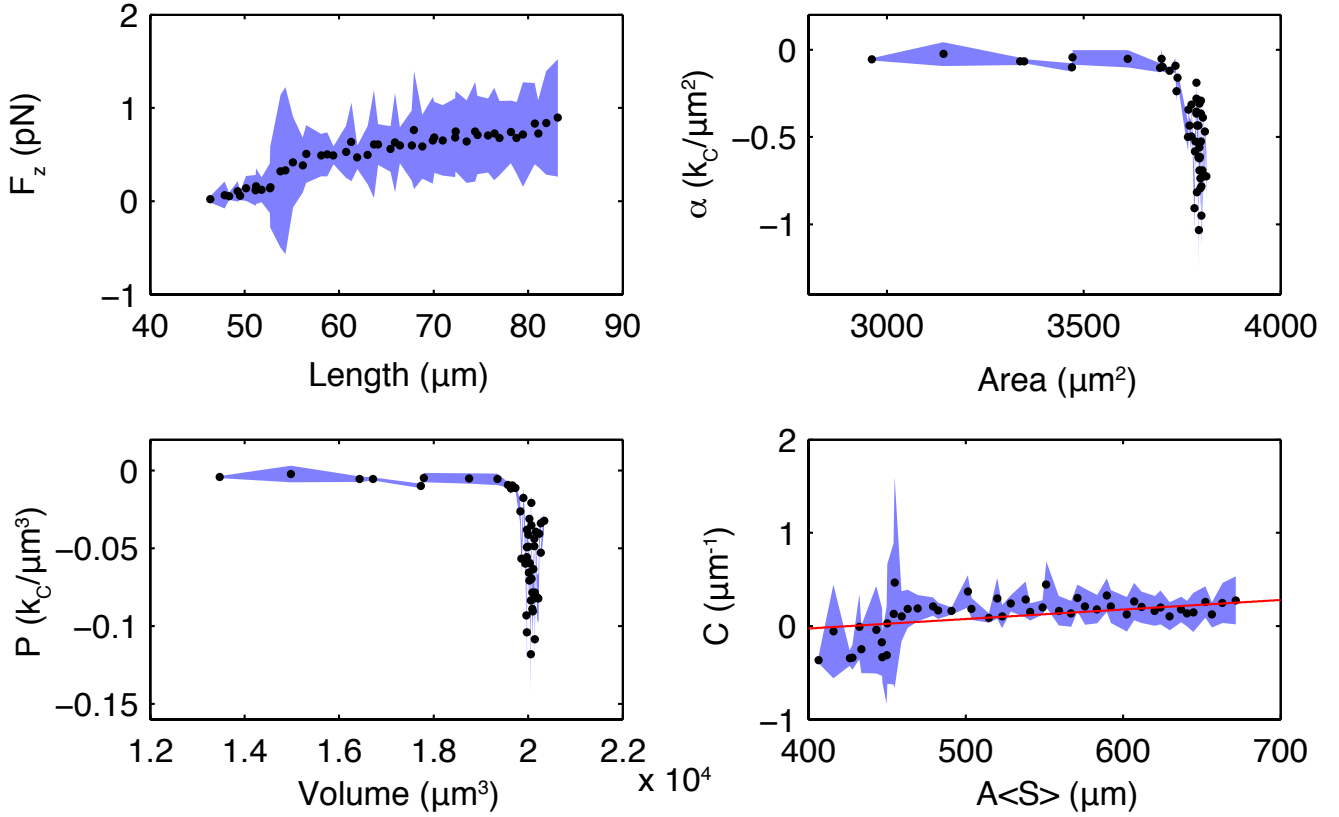


Figure S9: Effective constitutive relations for a tethered vesicle. In this figure we plot force versus length, tension versus area, pressure versus volume and spontaneous curvature versus integrated curvature for the vesicle shown in the main text. The black points indicate measured values and the blue regions show the corresponding errors in the ordinate variable. We note that the error in the right-most points on the tension and pressure plots, which appear here to be small and approximately constant, are actually dominated by the errors in area and volume, respectively, which are not shown. The predicted theoretical curve according to Eq. 30 (which did not require a fit) is shown in red for C versus integrated mean curvature.

1. Pressure and tension

At the beginning of the extension (the end of the retraction) in Fig. S8, there is a steep rise (drop) in the apparent volume and area of the membrane contradicting the claim that the vesicle volume and area are incompressible. This is entropically induced elasticity: although the actual volume and area of the membrane are nearly incompressible, some volume and area are hidden in the thermal membrane undulations. In Fig. S9, the fluctuation-dominated regime is clearly visible, corresponding to the “constant” tension and pressure regimes. In the high-tension limit, little membrane remains in membrane undulations and the tension and pressure can be interpreted as constraint forces. This regime is characterized by the constant area and volume at high tension as shown in Fig. S9.

2. Spontaneous curvature

The evolution of the spontaneous curvature is perhaps the least intuitive and understood of the Lagrange multipliers. The ADE theory predicts the dependence of spontaneous curvature on membrane deformation [6, 22, 23]:

$$C = -K_{\text{ADE}} (\langle S \rangle_{\mathcal{M}} - S_0), \quad (30)$$

where K_{ADE} is a non-local bending modulus and

$$\langle S \rangle_{\mathcal{M}} \equiv \mathcal{S}A^{-1} = A^{-1} \int_{\mathcal{M}} d^2\sigma S, \quad (31)$$

is the mean summed curvature over the deformed vesicle and S_0 is a constant. If the membrane is initially equilibrated by the slow processes of lipids flipping between leaflets, we would expect S_0 to be zero for the undeformed vesicle. In Fig. S9, this simple linear dependence on the mean summed curvature is not observed.

Unfortunately, there are a number of important considerations that may complicate the interpretation of the measured spontaneous curvature. (i) The relative error in the determination of the spontaneous curvature is larger than the other two Lagrange multipliers. (ii) In the fluctuation-dominated regime, the *Proximal Equilibrium Approximation* is problematic since the thermal undulations are large. Furthermore, the mean summed curvature reported in Fig. S9 does not account for the curvature in fluctuations, whereas mean summed curvature in Eq. 30 does include fluctuations. Like the membrane area, a considerable amount of the curvature is in membrane undulations at low tension. The summed mean curvature in the averaged conformation becomes more negative as the membrane is deformed, but as the tension is increased with membrane deformation, the curvature in undulations becomes less negative as it approaches zero. Therefore, the effect of entropy makes the interpretation of the dependence of the spontaneous curvature on the mean summed curvature problematic. (iii) Finally, there is also an important experimental consideration with regards to Eq. 30. This prediction depends on the assumption that the number of lipids in each bilayer is constant. Although the process of lipid transfer between leaflets is thought to be too slow to affect our experiments, all the vesicles in our experiments were functionalized and the osmotic pressure was lowered significantly, inducing budding transitions in many of the vesicles. These transitions may lead to defects in the membrane wall that could affect the lipid number either by allowing faster interchange between leaflets or by the opening of small, partially budded features on the membrane surface. Also, the effect of the optical bead interaction with the membrane cannot be ignored. In our experiments we observed the build up of fluorescence around the beads as the experiment progressed. While the fluorescent lipid may have originated from small vesicles in solution, it may also have been aggregated from the body if the vesicle itself, upsetting the fine balance of the lipid number in the body of the vesicle. Although it is difficult to draw any definite conclusions from the spontaneous curvature data, this data suggests that we may still not understand the nature of spontaneous curvature at physiological tensions.

B. Other extension series

In this section we present force measurements from other vesicles that were not included in the main text. In each plot, the red curve is the force measured from the optical trap and the blue curve represents the force measured from the conformation of the membrane using the Proximal Equilibrium Approximation.

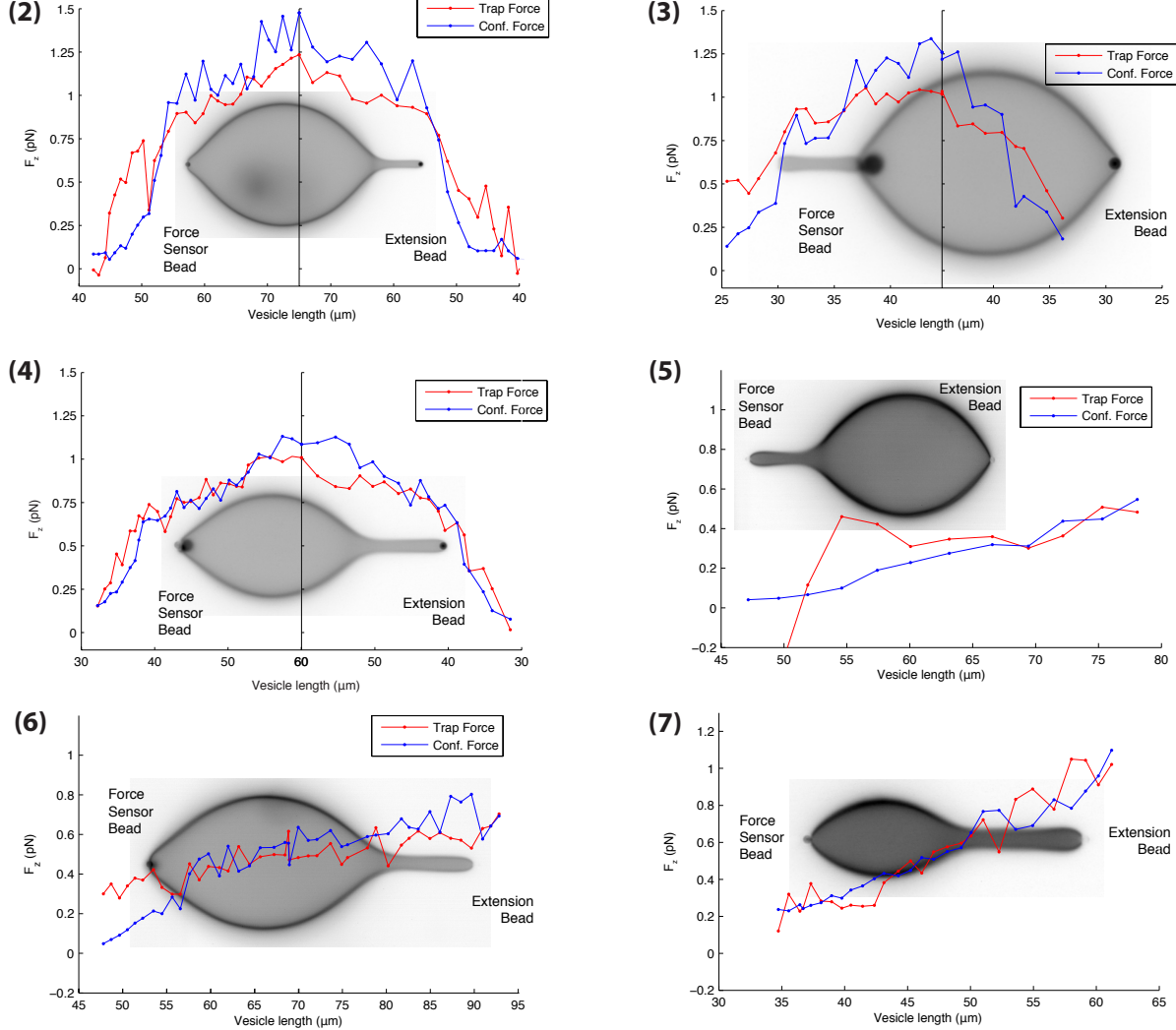


Figure S10: Data set 2: Anomalous forces due to light scattered by the membrane itself are apparent in the first few steps of this extension in the trap force; see Fig. S7 and discussion for more details. **Data set 3:** Anomalous forces due to light scattered by the membrane itself are apparent in the trap force. We found that data sets where the vesicles tethered on the extension side resulted in the best quantitative agreement with the conformational force. This is probably a result of the dramatic membrane conformational changes at the tethering pole which, in turn, lead to changes in the membrane induced scattering. **Data set 4:** This figure shows excellent agreement between the trap and conformational force. **Data set 5:** This figure shows an extreme example of the anomalous trapping forces induced by large-scale membrane conformational changes at the force sensor bead. **Data set 6:** This figure shows excellent agreement between the trap and conformational force for higher forces. **Data set 7:** This figure shows excellent agreement between the trap and conformational force.

-
- [1] W Helfrich. Elastic properties of lipid bilayers: theory and possible experiments. *Z. Naturforsch.*, 28(11):693–703, 1973.
- [2] P B Canham. The minimum energy of bending as a possible explanation of the biconcave shape of the human red blood cell. *J Theor Biol*, 26(1):61–81, 1970.
- [3] E A Evans. Bending resistance and chemically-induced moments in membrane bilayers. *Biophysical Journal*, 14:923–931, 1974.
- [4] W Rawicz, K C Olbrich, T McIntosh, D Needham, and E Evans. Effect of chain length and unsaturation on elasticity of lipid bilayers. *Biophys J*, 79(1):328–339, 2000.
- [5] Mikio Nakahara. *Geometry, topology, and physics*. Institute of Physics Publishing, 1990.
- [6] U. Seifert. Configurations of fluid membranes and vesicles. *Advances in Physics*, 46(1):13–137, Jan-Feb 1997.
- [7] J T Jenkins. Equations of mechanical equilibrium of a model membrane. *SIAM J. Appl. Math.*, 32(4):755–764, 1977.
- [8] J T Jenkins. Static equilibrium configurations of a model red blood cell. *J Math Biol*, 4(2):149–69, 1977.
- [9] D J Steigmann. Fluid films with curvature elasticity. *Archive for Rational Mechanics and Analysis*, 150(2):127–152, 1999.
- [10] OY Zhong-can and W Helfrich. Bending energy of vesicle membranes: General expressions for the first, second, and third variation of the shape energy and applications to spheres and cylinders. *Phys Rev A*, 39(10):5280–5288, 1989.
- [11] L D Landau and E M Lifshitz. *Theory of Elasticity*. Pergamon Press, 3rd English ed. revised and enlarged by E.M. Lifshitz, A.M. Kosevich, and L.P. Pitaevskii (soft) : edition, 1986.
- [12] R. Capovilla, J. Guven, and J. A. Santiago. Deformations of the geometry of lipid vesicles. *Journal of Physics A-Mathematical and General*, 36(23):6281–6295, Jun 2003.
- [13] R. Capovilla and J. Guven. Stress and geometry of lipid vesicles. *Journal of Physics-Condensed Matter*, 16(22):S2187–S2191, Jun 2004.
- [14] Martin Michael Muller, Markus Deserno, and Jemal Guven. Balancing torques in membrane-mediated interactions: exact results and numerical illustrations. *Phys Rev E Stat Nonlin Soft Matter Phys*, 76(1 Pt 1):011921, 2007.
- [15] Markus Deserno, Martin Michael Muller, and Jemal Guven. Contact lines for fluid surface adhesion. *Phys Rev E Stat Nonlin Soft Matter Phys*, 76(1 Pt 1):011605, 2007.
- [16] J. B. Fournier. On the stress and torque tensors in fluid membranes. *Soft Matter*, 3(7):883–888, 2007.
- [17] E Peterson, H J Lee, R Phillips, W Klug, and P Wiggins. In preparation.
- [18] T Baumgart, S Das, W W Webb, and J T Jenkins. Membrane elasticity in giant vesicles with fluid phase coexistence. *Biophys J*, 89(2):1067–1080, 2005 Aug.
- [19] V Heinrich, B Bozic, S Svetina, and B Zeks. Vesicle deformation by an axial load: from elongated shapes to tethered vesicles. *Biophys J*, 76(4):2056–71, 1999.
- [20] Arpita Upadhyaya and Michael P Sheetz. Tension in tubulovesicular networks of golgi and endoplasmic reticulum membranes. *Biophys J*, 86(5):2923–8, 2004.
- [21] Philip R Bevington and D. Keith Robinson. *Data reduction and error analysis for the physical sciences*. McGraw-Hill, 3rd edition, 2003.
- [22] R E Waugh, J Song, S Svetina, and B Zeks. Local and nonlocal curvature elasticity in bilayer membranes by tether formation from lecithin vesicles. *Biophys J*, 61(4):974–82, 1992.
- [23] L Miao, U Seifert, M Wortis, and HG Dobereiner. Budding transitions of fluid-bilayer vesicles: The effect of area-difference elasticity. *Physical Review E. Statistical Physics, Plasmas, Fluids, and Related Interdisciplinary Topics*, 49(6):5389–5407, 1994.